IEEE Access
Multidisciplinary ⋮ Rapid Review ⋮ Open Access Journal

Received 29 April 2023, accepted 16 May 2023, date of publication 24 May 2023, date of current version 13 June 2023.

Digital Object Identifier 10.1109/ACCESS.2023.3279765

RESEARCH ARTICLE

The Lorentz Group Using Conformal Geometric Algebra and Split Quaternions for Color Image Processing: Theory and Practice

EDUARDO BAYRO-CORROCHANO, (Senior Member, IEEE), ZULEIMA VAZQUEZ-FLORES, AND ULISES URIOSTEGUI-LEGORRETA

Department of Electrical Engineering and Computer Science, CINVESTAV, Campus Guadalajara, Jalisco 45119, Mexico

Corresponding author: Eduardo Bayro-Corrochano (eduardo.bayro@cinvestav.mx)

This work was supported by the Conacyt Project under Grant A1-S-10412.

ABSTRACT The processing of color images is of great interest, because the human perception of color is a very complex process, still not well understood. In this article, firstly the authors present an analysis of the well-known mathematical methods used to model color as a phenomenon and to process color images. We propose an adequate metric to process color images using the Minkowski or space-time metric. We propose that the processing of HSV images can be done using the HSV cone in the quaternion split algebra or the conformal geometric algebra frameworks. We show that the processing of RGB images using the Euclidean metric in the $\mathbb{R}^3$ doesn't yield good results. The colors of images change by daylight, we understand this phenomenon as the color change follows the action of the Lorentz Lie group. Consequently, we formulate a new model for representing and processing color using split quaternions and space-time conformal geometric algebra. We propose new algorithms for practical color image processing: we formulate the novel Split Quaternion Fourier Transform for color image processing and we interpolate color images using Split Motors which belong to the space-time conformal geometric algebra. The experimental part proves that real color images have to be processed in the HSV cone. We show successful applications of the Quaternion Split Fourier Transform and the interpolation processing. We compare these computations using the RGB metric in the $\mathbb{R}^3$ space and using the Minkowski metric in the HSV cone. This comparison shows clearly that the color image processing using the Minkowski metric in the HSV cone performs better.

INDEX TERMS Lorentz group transformation, conformal geometric algebra, split quaternions, Red Green Blue (RGB), Hue, Saturation, and Value (HSV), Quaternion Split Fourier Transform (QSFT), interpolation, color image processing.

I. INTRODUCTION

The development of a theory of color perception of the human color perception mechanisms is a longstanding problem addressed by the most influential figures of mathematical physics [18], [29], [42], [48]. One of the founding fathers of quantum mechanics, E. Schrödinger [42] contributes with his benchmark axiomatic work on color perception. H.L. Resnikoff [38] wrote an overview of the main historical contribution, where he points out that the space, which we denote by $\mathcal{C}$, of perceived colors is one of the very first examples of abstract manifold mentioned also by B. Riemann in his habilitation "Über die Hypothesen, Welche der Geometrie zu Grunde liegen" [39]. In 1853 the mathematician Grassmann stated the results of color mixture experiments in a form very similar to the assertion that the set of colors resides in a convex cone in 3-dimensional affine space. One year later, Riemann in 1854, in his Habilitationsschrift observed that *"the positions of the objects of sense and the colors, are probably the only familiar things whose specifications constitute multiply extended manifolds"*. This a meaningful remark whose implications remained hidden until Helmholtz brought them to light in 1891 [19].

Weyl [48] suggested characterizing the individual color perception as a specific correlative interaction between an abstract space of perceived colors and an embedding space

The associate editor coordinating the review of this manuscript and approving it for publication was Andrea F. Abate.

of physical colors. In the sense of Riemannian geometry, one can be tempted to define the space of perceived colors from basic largely accepted axioms. These axioms, which date back to the works of Grassmann and Von Helmholtz [18], [19] state that $\mathcal{C}$ is a regular convex cone of dimension 3. Note that convexity reflects the property which allows performing mixtures of perceived colors or in a quantum approach of color states [6].

In more recent years many authors wrote papers about color, to quote some: Weinberg [47] and Ashtekar [1]. According to Krantz [23] any Grassmann structure can be mapped homomorphically onto a convex cone in a vector space. This can be mathematically well established by three theorems for the Grassmann structure. In the sixties, Yilmaz [45], [46] had the advanced idea to point out the analogy between perceived colors theory and the special theory of relativity by observing that the saturation of spectral colors is not only an upper bound but also a perceptually invariant feature concerning the (broadband) illuminant used to light up a visual scene.

This clearly explains the analogy between this property of color saturation and the constancy of the speed of light in a vacuum measured by inertial observers. Yilmaz determined, based on three results from experiments, a law for the perceptual effect on color perception induced by a change of illuminant. Surprisingly, this law turns out to be the direct analogous of Lorentz transformations.

Based on this, he argued that a color space $\mathcal{C}$ endowed with a 3D Minkowski metric could be a valid alternative to the classical CIE colorimetric spaces, which are equipped with a Euclidean metric to measure perceived color distances.

Considering the axioms of Grassmann and Von Helmholtz [18], [19], one can see the space of perceived colors as a regular convex cone of real dimension 3. Resnikoff's main idea [36] enriches this model imposing that the cone of perceived colors is homogeneous.

Imposing one more property, namely self-duality, this cone becomes a symmetric cone [36]. The fundamental comment is that being symmetric the cone of perceived colors, it can be considered by Bertier [6] as the set of positive observables of a formally real Jordan algebra A [21]. For that, Bertier formulates the following trichromacy axiom: the Grassmann-Von Helmholtz cone of perceived colors is the positive cone of a formally real Jordan algebra of real dimension 3. This is precisely the statement of the famous Koecher-Vinberg theorem [2]. Since the cone is of real dimension 3, the algebra is also of real dimension 3. Using the classification theorem of Jordan, Von Neumann, and Wigner [21], one can check that the algebra A is necessarily isomorphic either to the Jordan algebra $\mathbb{R} \oplus \mathbb{R} \oplus \mathbb{R}$ or to the Jordan algebra H(2,$\mathbb{R}$) of symmetric real 2×2 matrices.

In consequence, adding the self-duality property, Resnikoff's classification stems from the classification theorem of Jordan, Von Neumann, and Wigner. Bertier formulates a trichromacy axiom as follows the Grassmann-Von Helmholtz cone of perceived colors is the positive cone of a formally real Jordan algebra [21] of real dimension 3. The Jordan algebra H(2,$\mathbb{R}$) can be considered as the non-associative algebra linearly spanned by the unit 1 and a spin system of the Clifford algebra of $\mathbb{R}^2$ [11], [31].

The Jordan algebra H(2,$\mathbb{R}$) carries a very special structure being isomorphic to the spin factor $\mathbb{R} \oplus \mathbb{R}^2$. It can be considered as the non-associative algebra linearly spanned by the unit 1 and a spin system of the Clifford algebra of $\mathbb{R}^2$ [11], [31].

Resnikoff [38] gave remarkable conclusions which he derives by adding the sole axiom, namely $\mathcal{C}$ is homogeneous under the action of the linear group of background illumination changes [36]. There are very few works devoted to the possible implications of hyperbolicity in color perception.

$\mathcal{C}$ is endowed with the rich structure of asymmetric cone [14]. Considering both this additional axiom, and the hypothesis that the distance on $\mathcal{C}$ is given by a Riemannian metric invariant under background illumination changes,. Resnikoff proposes that $\mathcal{C}$ can only be isomorphic to one of the two following Riemannian spaces: i) the product $\mathcal{C}_1 = \mathbb{R}^+ \times \mathbb{R}^+ \times \mathbb{R}^+$ equipped with a flat metric, precisely the Helmholtz–Stiles metric [49]; ii) $\mathcal{C}_2 = \mathbb{R}^+ \times SL(2,\mathbb{R})/SO(2,\mathbb{R})$ equipped with the Rao–Siegel metric of constant negative curvature, see [10] and [43]. Note that the quotient $SL(2,\mathbb{R})/SO(2,\mathbb{R})$ is isomorphic to the Poincaré hyperbolic disk D. Thus, one can infer that the first space is the usual metric space of the colorimetry, while the second one appears to be relevant to explain psychophysical phenomena such as the ones described by Yilmaz in [45], [46] or physiological mechanisms such as the neural coding of colors shown by Reinhard and De Valois [37], [44]. The geometry of the model $\mathcal{C}_2$ of H.L. Resnikoff is much richer than the geometry of the $\mathcal{C}_2$, however, there are very few works devoted to the possible implications of hyperbolicity in color perception.

Principe et al. [35] provide a mathematical formalization of Yilmaz's argument [45], [46] about the relationship between Lorentz transformations and the perceptual effect of illuminant changes. They explained that, within Yilmaz's model, the color space can be coherently endowed with the Minkowski metric only by imposing the Euclidean metric on the hue-chroma plane. The authors also show to what extent Yilmaz's model is related to the classical formulation of special relativity and what constraints $\mathcal{C}$ must satisfy to maximize the analogies between these two theories. Gogberashvili [17] shows how to adapt the almost forgotten work of Yilmaz about the relativity of color perception to perform a color correction of digital images through a three-dimensional version of Lorentz boosts used in the special theory of relativity. Bertier et al. [7] proposed a mathematical model by taking into account both trichromacy and color opponency. This permits us to explain theoretically the relativistic color perception phenomena argued by Yilmaz. Instead of relying directly on relativistic considerations,

TABLE 1. Analogies between special relativity and Yilmaz's model of color perception, table of [35].

Special Relativity	Yilmaz's Color Perception Model
Homogeneous and isotropic spacetime	Homogeneous and isotropic color space
Observer in an inertial frame	Observer adapted to a broadband illuminant
Event e = (t, x) $\in \mathbb{R}^4$	Perceived color $F = (\varphi, \rho, \gamma) \in \mathcal{C}$
Time coordinate t $\in \mathbb{R}$	Lightness coordinates $\gamma \in \mathbb{R}^+$
Spatial coordinates $(x_1, x_2, x_3) \in \mathbb{R}^3$	Chromatic coordinates $(\rho, \varphi) \in \mathbb{R}^+ \times [0, 2\pi)$
Speed of light in vacuum c	Maximal perceived saturation Σ
Lorentz transformations	Yilmaz transformations

Bertier et al. [7] base their theory on a quantum interpretation of color perception together with the trichromacy axiom, which summarizes well-established properties of trichromatic color vision within the framework of Jordan algebras. Table 1 of Prencipe et al. [35] shows analogies between special relativity and Yilmaz's model of color perception.

Furthermore, Bertier [6], [8] gives a quantum description of the space $\mathcal{C}_2$ of perceived colors. He shows that $\mathcal{C}_2$ is the effect space of a rebit (real quantum qubit), whose state space is isometric to Klein's hyperbolic disk $\mathcal{K}$, but its geodesics are visually very different, being the straight chords of the unit disk. Klein geometry appears naturally when considering the spin factor $\mathbb{R} \oplus \mathbb{R}^2$ and the 3-dimensional Minkowski future light cone $\mathcal{L}^+$ whose closure is the state cone of the rebit. He sustains that the chromatic state space S can be represented as a Bloch disk of real dimension 2 that coincides with the Hering disk given by the color opponency mechanism. This Bloch disk is an analog, in the real context, of the Bloch ball that describes the state space of a two-level quantum system of a spin- $\frac{1}{2}$ particle. Furthermore, he shows that the dynamics of this quantum system can be related to the color information processing that results from the activity rates of the four types of spectrally opponent cells [44]. Interestingly enough, the authors De Valois et al. [44] and Patterson et al. [34] show that spectrally opponent interactions in primates are usually considered to be performed by ganglion and lateral geniculate nucleus cells which are very similar concerning color processing.

In a different methodology as the Lie Groups-based algorithms, Discrete Hahn polynomials (DHPs) and their moments [28] are considered to be one of the efficient orthogonal moments and they are applied in image processing and feature extraction. Jassim et al. [27] introduced a new set of orthogonal polynomials and moments and the set's application in signal and image processing. This polynomial is derived from two well-known orthogonal polynomials: the Tchebichef and Krawtchouk polynomials.

In this article, we present a mathematical well-founded representation viewpoint of color theory. Our goal is to formulate the four Grassmann's laws for color in the geometric sub-algebra $G^+_{4,1}$ which has the correct pseudo-Euclidean space-time metric. This rotor sub-algebra is isomorph to the split quaternion algebra $\mathbb{H}_S$. We will show that this approach induces a formulation for holistic color processing opposite to the incorrect channel-wise processing approach. We will show that the appropriate Lie Group to model the group action caused by color change is the space-time Lorentz group or split motor $\boldsymbol{M}_s \in G_{4,1}$. In this formulation, the wedge product of the Clifford product intervenes in products between the color representations in terms of bivectors. Recent attempts for color image processing use the Quaternion Fourier Transform which uses a Euclidean metric. We will show, that the Lie group kernel of the Split Quaternion Fourier Transform (SQFT) for the correct color image transformation is an exponent of a Lorentz Lie algebra with the space-time pseudo-Euclidean metric. We show how one filters color images using the SQFT and how one can interpolate color images using the split motor algebra which is a sub-algebra of the conformal geometric algebra.

The contribution of this article is sustained by the following novel proposals,

- A new model for representing and processing color using split quaternions and space-time conformal geometric algebra
- Propose new algorithms for practical color image processing
  1) Formulate the novel Split Quaternion Fourier Transform for color image processing
  2) Interpolation of color images processing using Split Motors which belong to the space-time conformal geometric algebra

The paper structure is as follows: section II outlines geometric algebra, quaternion algebra, and motor algebra. Section III presents a mathematical well-founded representation viewpoint of color theory and the most important models for the color space using the HSV cone model, the trichromacy axiom, and the space-time metric for the Lorentz transformation. Section IV introduces the Quaternion Split Fourier Transform (QSFT) for color image processing. Section V shows the interpolation using Split Motors of the conformal geometric algebra $G_{4,1}$. Finally, section VI is devoted to the conclusion.

II. GEOMETRIC ALGEBRA, QUATERNION ALGEBRA, MOTOR ALGEBRA

A geometric algebra $\mathcal{G}_{p,q,r}$ is a lineal space of dimension 2^n, $n = p + q + r$, and $(p, q, r, \in \mathbb{N}$, where the p-vector basis squares to +1, the q-basis squares to -1, and the r-vector basis squares to 0. For a detailed explanation of the equations given in this section see [4].

A multivector consists of the linear combination of k-blades of different degrees. The Clifford product of A_r and B_s is

$$A_r B_s = \langle A_r B_s \rangle_{r+s} + \langle A_r B_s \rangle_{r+s-2} + \ldots + \langle A_r B_s \rangle_{|r-s|}\,, \tag{1}$$

where

$$A_r \cdot B_s = \langle A_r B_s \rangle_{|r-s|}\,, \tag{2}$$

$$A_r \wedge B_s = \langle A_r B_s \rangle_{r+s}\,. \tag{3}$$

A. PROPERTIES OF THE MULTIVECTORS

Given $A_r = \sum_{i=0}^{r} \langle A_r \rangle_i$, one can compute: the Clifford conjugation ($\overline{A}_r$), the reversion ($\widetilde{A}_r$), and the involution degree ($\widehat{A}_r$).

$$\overline{A}_r = \sum_{i=0}^{r} (-1)^{\frac{i(i+1)}{2}} \langle A_r \rangle_i \,, \tag{4}$$

$$\widetilde{A}_r = \sum_{i=0}^{r} (-1)^{\frac{i(i-1)}{2}} \langle A_r \rangle_i \,, \tag{5}$$

$$\widehat{A}_r = \sum_{i=0}^{r} (-1)^{i} \langle A_r \rangle_i \,. \tag{6}$$

The dual of a multivector A in $\mathcal{G}_n$ is computed as $A^* = A \cdot I_n^{-1}$. The *r-blade* is the dual of *(n-r)-blade*.
The exponential of a multivector A can be expressed as

$$exp(A) = \sum_{k=0}^{\infty} \frac{A^k}{k!}. \tag{7}$$

B. QUATERNION ALGEBRA

Quaternion numbers were discovered by William Hamilton in 1843. These numbers represent four-dimensional space and are composed of a real part and three imaginary parts.The four-dimensional quaternion algebra $\mathbb{H}$ [26] is associative, non-commutative

$$\mathbb{H} = \{\boldsymbol{q} = q_0 + q_x\boldsymbol{i} + q_y\boldsymbol{j} + q_z\boldsymbol{k} \;\; | q_o, q_x, q_y, q_z \in \mathbb{R}\}, \tag{8}$$

where the orthogonal imaginary numbers $\boldsymbol{i}, \boldsymbol{j}$, and $\boldsymbol{k}$ fulfill

$$\boldsymbol{i}^2 = \boldsymbol{j}^2 = -1, \;\; \boldsymbol{k} = \boldsymbol{ij} = -\boldsymbol{ji} \;\; \rightarrow \;\; \boldsymbol{k}^2 = -1. \tag{9}$$

A quaternion is conjugated as follows

$$\tilde{\boldsymbol{q}} = q_0 - q_x\boldsymbol{i} - q_y\boldsymbol{j} - q_z\boldsymbol{k}. \tag{10}$$

The modulus of the quaternion $\boldsymbol{q} = q_0 + q_x\boldsymbol{i} + q_y\boldsymbol{j} + q_z\boldsymbol{k}$ is defined by

$$|\boldsymbol{q}| = \sqrt{\boldsymbol{q}\tilde{\boldsymbol{q}}} = \sqrt{{q_0}^2 + {q_x}^2 + {q_y}^2 + {q_z}^2}. \tag{11}$$

Given $\boldsymbol{q}, \boldsymbol{p} \in \mathbb{H}$

$$\begin{aligned} |\boldsymbol{q}| &= |\tilde{\boldsymbol{q}}|, \text{ and } \widetilde{\boldsymbol{qp}} = \tilde{\boldsymbol{p}}\tilde{\boldsymbol{q}}, \\ |\boldsymbol{qp}| &= |\boldsymbol{pq}| = |\boldsymbol{q}||\boldsymbol{p}|, \\ |\boldsymbol{q} + \boldsymbol{p}| &\leq |\boldsymbol{q}| + |\boldsymbol{p}|. \end{aligned}$$

One computes the inverse of a quaternion $\boldsymbol{q} \neq 0$ as follows

$$\boldsymbol{q}^{-1} = \frac{\tilde{\boldsymbol{q}}}{|\boldsymbol{q}|^2}. \tag{12}$$

A pure quaternion is a quaternion with its scalar element zero $q_0 = 0$

$$\vec{\boldsymbol{q}} = q_x\boldsymbol{i} + q_y\boldsymbol{j} + q_z\boldsymbol{k}, \tag{13}$$

and a unit quaternion is given by

$$\boldsymbol{q}_u = s + x\boldsymbol{i} + y\boldsymbol{j} + z\boldsymbol{k}, \;\; \text{for } ||\boldsymbol{q}_u|| = 1. \tag{14}$$

The polar representation of a quaternion $\boldsymbol{q} = q_0 + q_x\boldsymbol{i} + q_y\boldsymbol{j} + q_z\boldsymbol{k}$ is

$$\boldsymbol{q} = |\boldsymbol{q}| e^{\boldsymbol{i}\phi} e^{\boldsymbol{k}\psi} e^{\boldsymbol{j}\theta}, \tag{15}$$

where the phase ranges are delimited as follows: $(\phi, \theta, \psi) \in [-\pi, \pi[\times[-\frac{\pi}{2}, \frac{\pi}{2}[\times[-\frac{\pi}{4}, \frac{\pi}{4}]$.

The product of a quaternion $\boldsymbol{q}$ and a scalar $\alpha \in \mathbb{R}$ is given by

$$\alpha\boldsymbol{q} = \alpha q_0 + \alpha q_x\boldsymbol{i} + \alpha q_y\boldsymbol{j} + \alpha q_z\boldsymbol{k}. \tag{16}$$

The addition and subtraction of two quaternions $\boldsymbol{q}$ and $\boldsymbol{p}$ is given by

$$\begin{aligned} \boldsymbol{r} &= r_0 + r = \boldsymbol{q} \pm \boldsymbol{p} \\ &= q_0 \pm p_0 + (q_x \pm p_x)\boldsymbol{i} + (q_y \pm p_y)\boldsymbol{j} + (q_{\pm} p_z)\boldsymbol{k}. \end{aligned} \tag{17}$$

The quaternionic product is given by

$$\begin{aligned} \boldsymbol{r} &= r_0 + r = \boldsymbol{pq} = (p_0 + p)(q_0 + q), \\ &= (p_0q_0 - p \cdot q) + (p_0p + q_0q + p \times q), \\ &= (p_0q_0 - p_xq_x - p_yq_y - p_zq_z) + \\ &\quad + (p_0q_x + p_xq_0 + p_yq_z - p_zq_y)\boldsymbol{i} + \\ &\quad + (p_0q_y - p_xq_z + p_yq_0 + p_zq_x)\boldsymbol{j} + \\ &\quad + (p_0q_z + p_xq_y - p_yq_x + p_zq_0)\boldsymbol{k}. \end{aligned} \tag{18}$$

C. SPLIT QUATERNION ALGEBRA

It is well known that quaternions represent rotations in 3D Euclidean and Minkowski spaces. In the latter, rotations are formulated with unit time-like quaternions in Minkowski 3-space [32]. The product by a quaternion gives rotation in two independent planes at once and obtains single-plane rotations. Ogberashvili [17] in his study of split quaternions and particles in (2+1)-space, explains that the double-cover property can be seen as a potential problem in the geometrical application of split quaternions, since (2+2)-the signature of their norms should not be changed for each product. If split quaternions form a proper algebraic structure for micro-physics, the representation of boosts in (2+1)-space leads to the interpretation of the scalar part of quaternions as a wavelength of particles. In our work, we will use the unit time-like quaternions in Minkowski 3-space.

In abstract algebra, the split-quaternions or coquaternions form an algebraic structure introduced by James Cockle in 1849 [33] under the latter name. They form an associative algebra of dimension four over the real numbers. Unlike quaternion algebra, split-quaternion algebra contains nontrivial zero divisors, nilpotent elements, and idempotents. That is why is called a non-division associative algebra.

The set of split quaternions is defined by

$$\mathbb{H}_S = \{\boldsymbol{q} = q_0 + q_x\boldsymbol{i} + q_y\boldsymbol{j} + q_z\boldsymbol{k} \;\; | q_o, q_x, q_y, q_z \in \mathbb{R}\}, \tag{19}$$

where the orthogonal imaginary numbers $\boldsymbol{i}, \boldsymbol{j}$, and $\boldsymbol{k}$ obey the following multiplicative rules:

$$\boldsymbol{i}^2 = \boldsymbol{j}^2 = 1, \;\; \boldsymbol{k}^2 = -1 \text{ and } \boldsymbol{ijk} = 1. \tag{20}$$

These relations imply $\boldsymbol{ij} = -\boldsymbol{ji} = \boldsymbol{k}, \boldsymbol{jk} = -\boldsymbol{kj} = -\boldsymbol{i}, \boldsymbol{ki} = -\boldsymbol{ik} = -\boldsymbol{j}$.

$$\begin{aligned}\boldsymbol{r} &= r_0 + r = \boldsymbol{pq} = (p_0 + p)(q_0 + q)\\ &= (p_0q_0 - p \cdot q) + (p_0p + q_0q + p \times q)\\ &= (p_0q_0 + p_xq_x + p_yq_y - p_zq_z)\\ &\quad + (p_0q_x + p_xq_0 + p_zq_y - p_yq_z)\boldsymbol{i}\\ &\quad + (p_0q_y + p_yq_0 + p_xq_z - p_zq_x)\boldsymbol{j}\\ &\quad + (p_0q_z + p_zq_0 - p_xq_y + p_yq_x)\boldsymbol{k}. \end{aligned} \tag{21}$$

The conjugate of a quaternion is given by

$$\tilde{\boldsymbol{q}} = q_s - q_x i - q_y j - q_z k. \tag{22}$$

The norm of the split quaternion $\boldsymbol{q} = q_0 + q_x\boldsymbol{i} + q_y\boldsymbol{j} + q_z\boldsymbol{k}$ is defined by

$$||\boldsymbol{q}|| = \sqrt{|\boldsymbol{q}\tilde{\boldsymbol{q}}|} = \sqrt{|{q_0}^2 - {q_x}^2 - {q_y}^2 + {q_z}^2|}. \tag{23}$$

Using the norm we can construct a unit quaternion:

$$\begin{aligned}\boldsymbol{q}_u &= \frac{\boldsymbol{q}}{||\boldsymbol{q}||},\\ ||\boldsymbol{q}_u|| &= 1. \end{aligned} \tag{24}$$

As nonzero split-quaternions are having a zero norm, split-quaternions form a "split composition algebra". A split-quaternion with a nonzero norm has a multiplicative inverse. The inverse of a split quaternion $\boldsymbol{q} \neq 0$ is given by

$$\boldsymbol{q}^{-1} = \frac{\tilde{\boldsymbol{q}}}{||\boldsymbol{q}||^2}, \tag{25}$$

Given

$$\begin{aligned}||\vec{\boldsymbol{q}}|| &= \sqrt{-q_x^2 - q_y^2 + q_z^2},\\ \hat{\boldsymbol{q}} &= \frac{q_x\boldsymbol{i} + q_y\boldsymbol{j} + q_z\boldsymbol{k}}{\sqrt{-q_x^2 - q_y^2 + q_z^2}}, \end{aligned} \tag{26}$$

the exponentiation of a split quaternion is

$$\begin{aligned}\exp^{\boldsymbol{q}} &= \exp^s \exp^{\vec{\boldsymbol{q}}} = \exp^s \exp^{\hat{\boldsymbol{q}}||\vec{\boldsymbol{q}}||},\\ &= \exp^s \left(\cos(||\vec{\boldsymbol{q}}||) + \hat{\boldsymbol{q}} \sin(||\vec{\boldsymbol{q}}||)\right). \end{aligned} \tag{27}$$

D. ROTORS IN G_3

The multivector basis of the 3D Euclidean space ($\mathcal{G}_{3,0,0} = \mathcal{G}_3$) is

$$\left\{ \underbrace{1}_{scalar}, \underbrace{e_1, e_2, e_3}_{vectors}, \underbrace{e_{23}, e_{31}, e_{12}}_{bivectors}, \underbrace{e_{123} \equiv I}_{trivectors} \right\}. \tag{28}$$

The rotors are expanded in terms of a bivector basis

$$\boldsymbol{R} = \underbrace{s}_{scalar} + \underbrace{xe_{23} + ye_{31} + ze_{12}}_{bivectors}, \tag{29}$$

$$\widetilde{\boldsymbol{R}} = \boldsymbol{R} = \underbrace{s}_{scalar} - \underbrace{xe_{23} - ye_{31} - ze_{12}}_{bivectors}, \tag{30}$$

where $s, x, y, z \in \mathbb{R}$ and $\boldsymbol{R}\widetilde{\boldsymbol{R}} = 1$.

A Rotor as operator represents the Lie Group $SO(3)$. Since a rotor is an isomorph to a quaternion, the following bivector relations are fulfilled

$$e_{23} = \boldsymbol{i}, \ e_{23} = -\boldsymbol{j}, \ e_{12} = \boldsymbol{k}, \tag{31}$$

where $\boldsymbol{i}, \boldsymbol{j}$, and $\boldsymbol{k} \in \mathbb{H}$. A rotor has a right-hand orientation whereas a quaternion has a left-hand.

The polar representation of a rotor reads

$$\boldsymbol{R} = exp\left(-\frac{\theta}{2}\boldsymbol{n}\right) = cos\left(\frac{\theta}{2}\right) - sen\left(\frac{\theta}{2}\right)\boldsymbol{n}, \tag{32}$$

where $\boldsymbol{n}$ is a unit bivector that represents the rotation plane and $\theta \in \mathbb{R}$ represents the rotation angle.

E. MOTORS IN $G_{3,1}$

The multivector basis of $G_{3,1}$ is given by as shown in the equation at the bottom of the next page, where $e_i^2 = 1$, $i = 1, 2, 3$, $e_4^2 = -1$. The $I_p = e_{1234}$ is the Pseudoscalar which $I_p^2 = -1$. For a detailed treatment of motor algebra see [4].

The pair $(\mathbb{R}^{3,1}, \langle\rangle)$ formed by the vector $\mathbb{R}^{3,1}$ and the Minkowski metric is called the Minkowski space or Minkowski spacetime. The spacetime interval between two events in Minkowski space is either:

1) Space-like,
2) Light-like ('null') or,
3) Time-like.

Considering $\{e_1, e_2, e_3, e_4\}$ the basis of $G_{3,1}(\mathbb{R}^4)$. The elements $\langle e_i, e_j\rangle$ form the matrix and its signature represents the Minkowski metric in:

$$Q = \begin{bmatrix} 1 & 0 & 0 & 0\\ 0 & 1 & 0 & 0\\ 0 & 0 & 1 & 0\\ 0 & 0 & 0 & -1 \end{bmatrix} \tag{33}$$

this allows to write the metric matrix; given $x = x_1e_1 + x_2e_2 + x_3e_3 + x_4e_4$, $y = y_1e_1 + y_2e_2 + y_3e_3 + y_4e_4$ the inner product $\langle x, y\rangle$ is

$$\langle x, y\rangle = x^t Qy \tag{34}$$

for all $x, y \in G_3, 1(\mathbb{R}^4)$, where in matrix writing the written vectors are always interpreted as their column components. Let $v \in G_{3,1}(\mathbb{R}^4)$, see Figure 1,

1) v is called a space vector, if $\langle v, v\rangle > 0$,
2) v is called the light vector, if $\langle v, v\rangle = 0$,
3) v is called a time vector, if $\langle v, v\rangle < 0$.

The norm of a vector is defined as $|v| = \sqrt{|\langle v, v\rangle|}$ which always exists and is greater than or equal to zero, but the light vectors are not null and have zero norms.

In projective geometry, homographies represent projective, affine, similitude, and Euclidean transformations. The projective transformations of points, lines, and planes are carried out

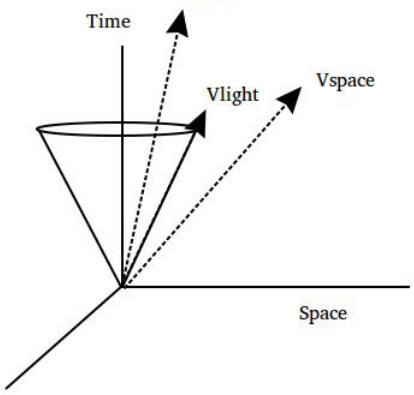

FIGURE 1. Light cone: Vtime is a time vector, Vlight is a light vector, and Vspace is a space vector.

using the following motor

$$\begin{aligned} \boldsymbol{M} = \boldsymbol{T}\boldsymbol{R}_S &= (1 + I_p\frac{\boldsymbol{t}}{2})\boldsymbol{R} = \boldsymbol{R} + I_p R', \\ &= s + r_x e_{23} + r_y e_{31} + r_z e_{12} + \\ &\quad + s' I_p + r'_x e_{41} + r'_y e_{42} + r'_z e_{43}, \\ &= s + r_x e_{23} + r_y e_{31} + r_z e_{12} + \\ &\quad + I_p(s' + r'_x e_{23} + r'_y e_{31} + r'_z e_{12}). \end{aligned} \tag{35}$$

The motor transformation leaves the point at infinity invariant. Since the $I_p^2 = -1$ the signature of the space corresponds to the Minkowski space-time metric and this motor is a complex rotor isomorph to a complex quaternion. The projective motion of a line expressed in Plucker coordinates reads

$$\boldsymbol{L}' = \boldsymbol{M}\boldsymbol{L}\widetilde{\boldsymbol{M}} = \boldsymbol{M}(\boldsymbol{m} + I_p\boldsymbol{n})\,\widetilde{\boldsymbol{M}}, \tag{36}$$

where $\boldsymbol{m}, \boldsymbol{n}$ stands for the moment and orientation of the line $\boldsymbol{L}$.

F. MOTORS IN $G^+_{3,0,1}$

A Euclidean transformation includes both rotation and translation, which are represented by a motor that belongs to the motor algebra $\mathcal{G}^+_{3,0,1}$. A motor as a linear operator represents the Lie Group $SE(3)$ and

A general rotor is given by expressing Eq. 32

$$\boldsymbol{R} = e^{-\frac{1}{2}L\theta} = cos(\theta/2) + sin(\theta/2)\boldsymbol{L}. \tag{37}$$

where the screw axis line is $\boldsymbol{L} = \boldsymbol{n} + I\boldsymbol{m}$, $\boldsymbol{n}$ (orientation) and $\boldsymbol{m}$ (moment).

The translator is given by

$$T = \boldsymbol{T} = (1 + I\frac{\boldsymbol{t}}{2}), \tag{38}$$

where the translation $\boldsymbol{t} = t_1e_1 + t_2e_2 + t_3e_3$ is in $\mathbb{R}^3$. The screw motion can be represented via a motor which in turn consists of the geometric product of a translator $\boldsymbol{T}$ and a rotor $\boldsymbol{R}$

$$\boldsymbol{M} = \boldsymbol{T}\boldsymbol{R} \tag{39}$$

for an arbitrary axis $\boldsymbol{L}$, and is applied to a geometric entity Q as follows:

$$Q' = \boldsymbol{T}\boldsymbol{R}Q\widetilde{\boldsymbol{R}}\widetilde{\boldsymbol{T}}. \tag{40}$$

Another representation of a motor follows

$$\boldsymbol{M} = \boldsymbol{T}\boldsymbol{R} = \boldsymbol{R} + I\boldsymbol{R}' = (a_0 + \boldsymbol{a}) + I(b_0 + \boldsymbol{b}). \tag{41}$$

G. SPLIT ROTORS AND SPLIT MOTORS IN CONFORMAL GEOMETRIC ALGEBRA A MOTOR BELONGS TO $\mathcal{G}^+_{3,0,1}$

The $\mathcal{G}^+_{3,0,1}$ has an orthonormal vector basis given by $\{e_1, e_2, e_2, e_4, e_5\}$ with the properties $e_i^2 = 1, \;\; i = 1, 2, 3$, $e_4^2 = 1, e_5^2 = -1, e_i \cdot e_4 = e_i \cdot e_5 = e_4 \cdot e_5 = 0, \;\; i = 1, 2, 3$.

The *null basis* $\{e_0, e_\infty\}$ seen as origin and point at infinity respectively, are defined as

$$e_0 = \frac{(e_5 - e_4)}{2}, \qquad e_\infty = e_4 + e_5. \tag{42}$$

These null vectors satisfy the properties $e_0^2 = e_\infty^2 = 0$ and $e_\infty \cdot e_0 = -1$.

$\boldsymbol{E} = e_\infty \wedge e_0$ is the Minkowski plane. Given a nonsingular k-vector $\boldsymbol{A} \in G_{4,1}$ with signature $\{p = 4, q = 1, r = 0\}$the dual and its inverse are respectively

$$\boldsymbol{A}^* = AI_c \;\; and \;\; \boldsymbol{A}^{-1} = \{-1\}^q \frac{\boldsymbol{A}^\dagger}{|\boldsymbol{A}|^2}, \tag{43}$$

where $\boldsymbol{A}^\dagger$ stands for the reversion of $\boldsymbol{A}$ and $|\boldsymbol{A}|$ its magnitude. For a detailed treatment of conformal geometric algebra see [3] and [4]. Lorentz group denoted $SL(2, \mathbb{C})$ preserves the orientation of space and direction of time. The Lorentz group is isomorph to the split motor given by

$$\boldsymbol{M}_s = \boldsymbol{R}_s\boldsymbol{T}. \tag{44}$$

This kind of motor carries out a screw motion in space and time, i.e. has a Minkowski metric. Different from the Euclidean rotor, a split rotor is spanned as follows

$$\boldsymbol{R}_S = \underbrace{s}_{scalar} + \underbrace{xe_{15} + ye_{25} + ze_{12}}_{bivectors}, \tag{45}$$

where $e_{15}^2 = 1, e_{25}^2 = 1, e_{12}^2 = -1$. Thus the split motor is given by the geometric product of a translator and split rotor

$$\boldsymbol{M}_S = \boldsymbol{T}\boldsymbol{R}_S = (1 + e_\infty\frac{\boldsymbol{t}}{2})\boldsymbol{R}_S = \boldsymbol{R}_S + e_\infty \boldsymbol{R}'_S. \tag{46}$$

Note that instead of the Pseudoscalar of the motor algebra I which $I^2 = 0$, we use the null vector e_∞ which $e_\infty^2 = 0$,

$$\{\underbrace{1}_{scale}, \underbrace{e_1, e_2, e_3, e_4}_{vectors}, \underbrace{e_{23}, e_{31}, e_{12}, e_{41}, e_{42}, e_{43}}_{bivectores}, \underbrace{e_{123}, e_{124}, e_{134}, e_{234}}_{trivectors}, e_{1234}\}$$

because both the motor and split motor are dual rotors. Thus, we can affirm that a motor is isomorph with a dual quaternion and a split motor is isomorph with a split dual quaternion. Furthermore, biquaternions and split motors are isomorphic to $SL(2, C)$.

The motor (Lie Group $SE(3)$) preserves isometries of the 3D Euclidean space and leaves the origin fixed. Motors induce a linear screw motion along a line in the 3D space. Whereas the split motor (Lorentz group $SL(2, \mathbb{C})$) is a subgroup of the Poincaré group (group of all isometries of Minkowski spacetime).

Summarizing the different analyzed motors:

i) dual rotor in motor algebra $G^{+}_{3,1,0}$ isomorph to a dual quaternion

$\boldsymbol{M} = \boldsymbol{R} + I\boldsymbol{R}' \equiv \boldsymbol{q} + \epsilon\boldsymbol{q}'$, $I^2 = \epsilon^2 = 0$, where $\boldsymbol{R} = s + xe_{23} + ye_{31} + ze_{12}$.

ii) hyperbolic (double) rotor in $G_{3,1}$ isomorph to double quaternion

$\boldsymbol{M} = \boldsymbol{R} + I_p\boldsymbol{R}' \equiv \boldsymbol{q} + \epsilon\boldsymbol{q}'$, $I_p^2 = \epsilon^2 = 1$,

iii) dual rotor in $G_{4,1}$ isomorph to dual quaternion

$\boldsymbol{M} = \boldsymbol{R} + e_\infty\boldsymbol{R}' \equiv \boldsymbol{q} + \epsilon\boldsymbol{q}'$ $e_\infty^2 = \epsilon^2 = 0$,

iv) dual split motor in $G_{4,1}$ dual split quaternion

$\boldsymbol{M} = \boldsymbol{R}_S + e_\infty\boldsymbol{R}'_S \equiv \boldsymbol{q}_s + \epsilon\boldsymbol{q}'_s$ $e_\infty^2 = \epsilon^2 = 0$, where $\boldsymbol{R}_S = s + xe_{15} + ye_{25} + ze_{12}$.

III. THE REPRESENTATIONAL VIEWPOINT IN COLOR THEORY

In this section, we present a mathematical well-founded representation viewpoint of color theory. Firstly, we will review the well-known attempts and improve them with our formulation. Our goal is to formulate the four Grassmann's laws for color in the geometric sub-algebra $G^{+}_{4.1}$ which has the correct pseudo-Euclidean space-time metric. This rotor sub-algebra is isomorph to the split quaternion algebra $\mathbb{H}_S$. We will show that this approach induces a formulation for holistic color processing opposite to the incorrect channel-wise processing approach. Recent attempts for color image processing use the Quaternion Fourier Transform which uses a Euclidean metric. We will show that the appropriate Lie Group to model the group action caused by color change is the space-time Lorentz group or split motor $\boldsymbol{M}_s \in G_{4.1}$. In this formulation, the wedge product of the Clifford product intervenes in products between the color representations in terms of bivectors. Moreover, the Lie group kernel of the Split Quaternion FFT for the correct color image transformation is an exponent of a Lorentz Lie algebra with the space-time pseudo-Euclidean metric.

A. COLOR MODELS

According to the literature [24], [49], there is not a single and simple 3D vector space that accurately predicts human visual perception. Depending on the applications, it needs n-dimensions, to take into account the many factors of our complex visual system. Other relevant aspects of visual perception of light and color include stimulus size, spatial frequency, light adaptation, local adaptation, contrast adaptation, surround effects, Helmholtz Kohlrausch effects, etc. Considering these aspects, the dimension n of space will increase, and as a model will be impractical.

A color model is an abstract mathematical model which describes the way colors can be represented as tuples of numbers, for example, triples in RGB or quadruples in CMYK. Gamma-encoded RGB spaces are probably not ideal for vector mathematics, that is, the Euclidean distances will not be uniform either for light or human perception. Specifically, the linearized RGB and CIEXYZ would be vector spaces, with their values relative to light in the scene or real-world; but not uniform relative to human perception. Color spaces like LAB, LUV, etc. are substantially more usable as a vector space if one wants distances to be relative to perception, i.e. perceptually uniform. But these models for uniformity, unfortunately, do not involve many of the aspects of human visual perception. Authors proposed more complex models, such as the Hunt model, CIECAM02, CAM16, ICAM, and others which take into account extra features to predict better visual perception.

The CIE color model uses tristimulus a combination of 3 color values that are close to the values red, green, and blue, which are mapped on a 3D space. One expects that by combing these values, one can reproduce any color that a human eye can perceive. The authors of the CIE specification claim that their model can represent accurately every single color the human eye can perceive.

Red Green Blue (RGB) describes the chromaticity component of a given color when excluding luminance. RGB itself is not a color space, it is a color model. Many different color spaces utilize this color model to describe their chromaticities because the R, G, and B chromaticities are one facet of reproducing color in CRT and LED displays.

In the cases of the analog YUV and digital YCbCr, they belong to a variety of linear methods, which using linear combination try to separate lightness from chroma signals in an RGB input.

When the input RGB values are gamma-corrected, this separation does not truly yield truly lightness and two chroma signals, but it produces instead a luma signal and two chrominance signals. YUV is originally utilized in video, because human eyes have less resolution in their color perception, thus it is more economical to put more of the bandwidth into encoding Luma. In the case of YCC, separating also has the added benefit of removing most of the correlation between the input channels, as a result, it provides a better compression.

HSV (hue, saturation, value) and HSL are transformations of Cartesian RGB primaries (usually sRGB), and their components and colorimetry are relative to the colorspace from which they are derived. HSV also known as HSB (hue, saturation, brightness), is often utilized by artists, because it appears more natural to think and handle color in terms of hue and saturation than in terms of the subtraction or addition of color components. Concluding, the HSV and HSL models do not effectively separate color into their three value components according to human perception of color.

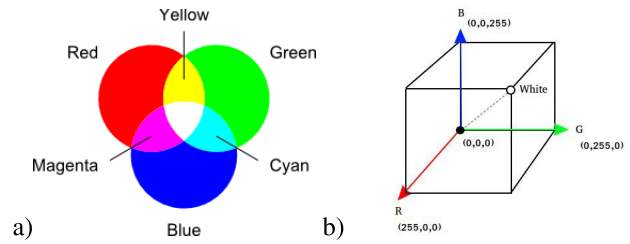

FIGURE 2. RGB model: a) color additive model, b)color space in the shape of a cube.

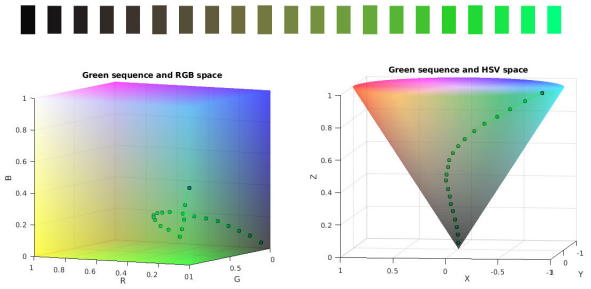

FIGURE 3. Changes of pixel colors from black to blue represented in: b) in $\mathbb{R}^3$, c) in the HSV cone model.

In this study, we select among many color models, the RGB model and the HSV model as they are of common use and intrinsically different for RGB one uses Euclidean metric and for the HSV model cone one uses Minkowski metric. Since we are focusing on the role of the metric, we will study only the RGB and HSV and in the experimental part compare their algorithms.

B. GRASSMAN'S LAWS

The fundamental properties of *metameric* color matching $\sim$ together with $\oplus$ and $*$ were introduced by Grassmann (1853-4) [18].

1) Law of equivalence. $\sim$ is an equivalence relation of S, $\forall,\ u, v, w \in S$:
   a) $u \sim u$;
   b) if $u \sim v$, then $v \sim u$;
   c) if $u \sim v$ and $v \sim w$, then $u \sim w$.
2) Law of additivity. $\forall,\ u, v, w \in S$, $u \sim v$ if and only if $u \oplus w \sim v \oplus w$.
3) Law of scalar multiplication. $\forall,\ u, v \in S$ and $t \in \mathbb{R}^+$, if $u \sim v$, then $t * u \sim t * v$.
4) Law of trichromacy.
   a) For any $u_0, u_1, u_2.u_3 \in S$ there exist positive number numbers $t_i, s_i,\ i = 0, 1, 2, 3$ such that $t_i \neq s_i$ for at least one i, and such that
   $$\sum_{i=0}^{3} t_i * u_i \sim \sum_{i=0}^{3} s_i * u_i, \tag{47}$$
   note that we use $\sum$ for sums involving *oplus*.
   b) There exists $u_1, u_2, u_3 \in S$ such that for any positive $t_i, s_i, i = 1, 2, 3$, if
   $$\sum_{i=0}^{3} t_i * u_i \sim \sum_{i=0}^{3} s_i * u_i,$$
   $$\texttt{then}\ t_i = s_i\ \texttt{for}\ i = 1, 2, 3. \tag{48}$$

C. REPRESENTATION OF GRASSMANN STRUCTURES USING QUATERNION ALGEBRA $\mathbb{H}$ FOR THE COLOUR MODEL RGB

The model of RGB defines the color space as a Cartesian system (Euclidean coordinates) where the reference bases are the colors red (Red), green (Green), and blue (Blue), expressed as orthogonal vectors. It is based on additive synthesis, in which the different colors are formed from the mixture of the three primary colors, see Figure 2.a.

Normally, the mathematical representation is defined with an intensity between 0 and 255 for each base color, allowing 256 different tones to be created. The combination of the three with their intensity variants offers a palette of more than 16 million colors. As a result, a color space in the shape of a cube is generated, where each color is defined within this cube. According to this RGB model, the absence of light (black) is located at the coordinates (0, 0, 0), and at the opposite vertex (255, 255, 255) is located the white that represents the mixture of all the colors according to the synthesis additive. The diagonal line that joins both vertices symbolizes the grayscale. The primary and secondary colors are located at the remaining vertices of the cube, see Figure 2.b.

A representation of color theory using the 3D space with Euclidean metric does fulfill Grassman's Laws given in subsection III-B. According to Theorem 3, the vector space is three-dimensional if and only if $< S, \oplus, *, \sim >$ is 3-chromatic.

This representation is the most popular way to represent the color pixels of a color image, namely

$$\vec{p}(x, y) = Re_1 + Ge_2 + Be_3 \in \mathbb{R}^3. \tag{49}$$

On the other hand, some researchers [40], [41] choose a pure quaternions $\vec{q} \in \mathbb{H}$ with Euclidean metric in a space $\mathbb{R}^4$ to represent the pixels of color images, namely

$$\vec{q}(x, y) = R\boldsymbol{i} + G\boldsymbol{j} + B\boldsymbol{k} \in \mathbb{H}. \tag{50}$$

We experimented to observe how we perceive color changes when daylight changes during the day, as shown in a pixel sequence in Figure 3.a. We noticed that the color vector $\vec{p(t)}(x, y)$ of a pixel moves in the RGB 3D space showing not a smooth path, rather the points are dispersed without a clear motion path, as it shown in Figure 3.a. In contrast, the changes of the pixel color in the HSV cone model move in a smooth path as shown in Figure 3.b.

When we observed this behavior of the pixels while the daylight is changing, we suspected that the use of the 3D Euclidean space for representing the color is not correct. We claim that here the metric of space has to be pseudo-Euclidean. Many authors [6], [18], [19], [35], [38], [45]

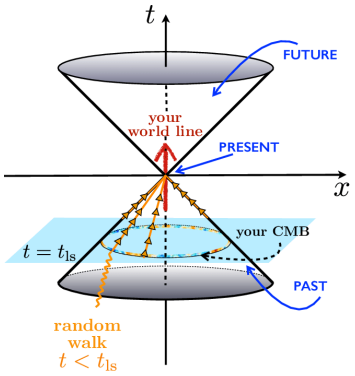

FIGURE 4. The light cone used in the theory of relativity.

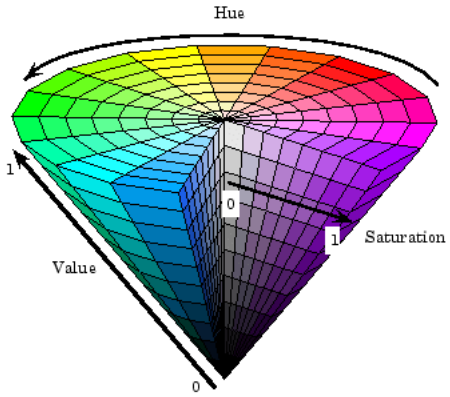

FIGURE 5. HSV cone model.

proposed that any Grassmann structure can be mapped homomorphically onto a convex cone in a vector space involving a space-time Minkowski metric and the Lorenz group. This precise suggestion leads us to choose instead the HSV cone model to represent the color and the split quaternions and a space-time conformal geometric algebra $G_{4,1}$. This is explained in the next subsection.

D. REPRESENTATION OF GRASSMANN STRUCTURES USING QUATERNION SPLIT ALGEBRA $\mathbb{H}_S$ FOR THE COLOR MODEL HSV

The HSV color space is a three-dimensional representation of color based on the components of hue, saturation, and brightness, defined in 1978 by Alvy Ray Smith [9]. The color space that this model creates is a cone based on the Hue, Saturation, and Value (HSV) given by

- Hue is represented by an angle around a vertical axis ($°0,\ldots,°360$).
- Saturation ranges from 0 to 1. Represents the purity of a hue. The maximum is represented with $S = 1$, while with $S = 0$ we have the grayscale.
- The Value ranges from 0 to 1. Zero stands at the bottom of the pyramid and represents black. The maximum value 1 corresponds to the top of the pyramid, with white in the center and pure shades on the perimeter since they are colors with $V = 1$ and $S = 1$ as depicted in Figure 5. The color points are confined in the cone with an upper bound of value $V = 1$. In contrast, in the light-cone model used in relativity, the boosts do have not a bound and move in the future light cone as shown in Figure 4.

The equations that relate the components of the HSV model to those of the RGB model are, see Figure 5

$$\begin{aligned} H &= \cos^{-1}\left(\frac{0.5[(R-G)+(R+G)]}{\sqrt{[(R-G)^2+(R-B)(G-B)]}}\right) \\ S &= 1 - \frac{3[min(R,G,B)]}{R+G+B} \\ V &= max(R,G,B). \end{aligned} \tag{51}$$

A representation of color theory using the HSV color space mapped onto a convex cone can be done using the split quaternions which have a space-time Minwosky metric, so the space has pseudo-Euclidean metric $\mathbb{R}^{3,1}$.

$$\vec{\boldsymbol{q}}(x,y) = H\boldsymbol{i} + S\boldsymbol{j} + V\boldsymbol{k} \in \mathbb{H}_S,\ H,S,V \in \mathbb{R}, \tag{52}$$

where $\boldsymbol{q} \in \mathbb{H}_S$. A Color pixel changes its color when the daylight changes during the day. We observed that at the cone the color vector $\boldsymbol{q}(x,y,z)$ moves following a smooth path, as shown in 3.b. The space $\mathbb{R}^{3,1}$ has Minkowski space-time metric, so we can reckon that the Lie group operator that causes the motion of a color point is the Lorentz group, which is an isotropy subgroup of the isometry group of Minkowski spacetime.

Following the ideas the authors reviewed in the introduction, the main contribution of this article is to use the correct Lie group which acts on the color visual manifold of the color. As a result, the correct representation of color points can be done using the split quaternions of $\mathbb{H}_S(\mathbb{R}^{3,1})$. Thus, the established use of quaternions of $\mathbb{H}(\mathbb{R}^4)$ for color space representation is wrong. Next section, we will present applications of image processing using this new representation in terms of the split quaternions. We show applications of the Split Quaternion FFT and the interpolation of color images under changes of illumination using the split motor (Lorentz group $SL(2,\mathbb{C})$).

IV. COLOUR IMAGE PROCESSING USING THE QUATERNION SPLIT FAST FOURIER TRANSFORM

The Quaternion Fourier Transform (QFT) has been used to process RGB color images [40]. The three components R, G, and B of the color image are encoded in a pure quaternion

$$q = Ri + Gk + Bk. \tag{53}$$

The kernel of the QFT uses an Euclidean metric. In this paper we use the quaternion split algebra to process HSV color images using the Minkowski metric. The three components H, S, and V of the color image are encoded in a pure quaternion

$$q = Hi + Sk + Vk. \tag{54}$$

A. QUATERNION SPLIT FAST FOURIER TRANSFORM

The inverse of a quaternion $\mu \in \mathbb{H}_S$ is computed in terms of its conjugated and norm as follows

$$\begin{aligned} \mu &= a + bi + cj + dk, \\ \tilde{\mu} &= a - bi - cj - dk, \\ ||\mu|| &= \sqrt{\mu\tilde{\mu}} = \sqrt{a^2 - b^2 - c^2 + d^2} \\ \hat{\mu} &= \frac{\mu}{||\mu||}. \end{aligned} \tag{55}$$

A unit pure quaternion ($a = 0$) is given by

$$\hat{\mu} = \frac{bi + cj + dk}{||\vec{\mu}||} = \frac{bi + cj + dk}{\sqrt{-b^2 - c^2 + d^2}}. \tag{56}$$

And the exponentiation of a quaternion is given by

$$\begin{aligned} \exp^{\mu} &= \exp^{a} \exp^{\vec{\mu}} = \exp^{a} \exp^{\hat{\mu}||\vec{\mu}||}, \\ &\exp^{a}[\cos(||\vec{\mu}||) + \hat{\mu}\sin(||\vec{\mu}||)]. \end{aligned} \tag{57}$$

To construct the quaternion Fourier transform with the Minkowski metric, we consider the exponentiation of a unit quaternion (57) whit $a = 0$. The color image is represented as a split quaternion $q(i,j) = H(i,j)\boldsymbol{i} + S(i,j)\boldsymbol{j} + V(i.j)\boldsymbol{k} \in \mathbb{H}_S$. Because the multiplication between quaternions is not commutative, one can compute three quaternions Fourier transforms of a color image, namely

$$\mathcal{F}^{\pm L}[q] = \frac{1}{\sqrt{MN}} \sum_{m=0}^{M-1} \sum_{n=0}^{N-1} \exp^{\mp\mu 2\pi(mv/M + nu/N)} q, \tag{58}$$

$$\mathcal{F}^{\pm R}[q] = \frac{1}{\sqrt{MN}} \sum_{m=0}^{M-1} \sum_{n=0}^{N-1} q \exp^{\mp\mu 2\pi(mv/M + nu/N)}, \tag{59}$$

$$\mathcal{F}^{\pm M}[q] = \frac{1}{\sqrt{MN}} \sum_{m=0}^{M-1} \sum_{n=0}^{N-1} \exp^{\mp\mu 2\pi mv/M} q \exp^{\mp\mu 2\pi nu/N}. \tag{60}$$

Figure 6 shows the quaternion split Fourier transform (QSFT) and its inverse and Figure 7 shows the quaternion Fourier transform with the Euclidean metric and its inverse.

B. SYMPLECTIC FORM OF THE QUATERNION

We encode the three components of the color image in a pure quaternion

$$q = Hi + Sk + Vk, \tag{61}$$

this avoids processing each component of the color image separately and working with the image like a single entity. We can write a quaternion using the Cayley-Dickson form [13], that consists in representing the quaternion only with two basic elements $\boldsymbol{i}$ and $\boldsymbol{j}$, as

$$Q = A + Bj = Hi + (S + Vi)\boldsymbol{j} \tag{62}$$

with this representation is possible to construct the symplectic form [20] of an image as follows

$$Q'_s = A' + B'\mu_2 = (H'\mu_1) + (S' + V'\mu_1)\mu_2, \tag{63}$$

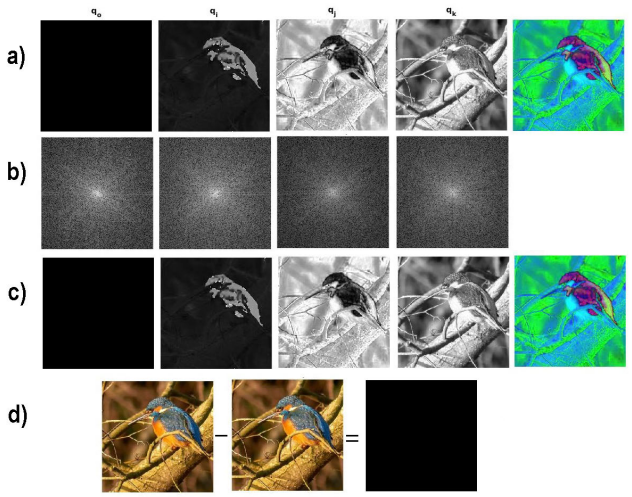

FIGURE 6. Quaternion split Fourier transform (QSFT) and its inverse of a quaternion image: a) the quaternion image and the original image; b) QSFT; c) the inverse of QSFT and the reconstructed image via the inverse of the QSFT; d) the subtraction between the original image and the reconstructed image via the inverse of QSFT.

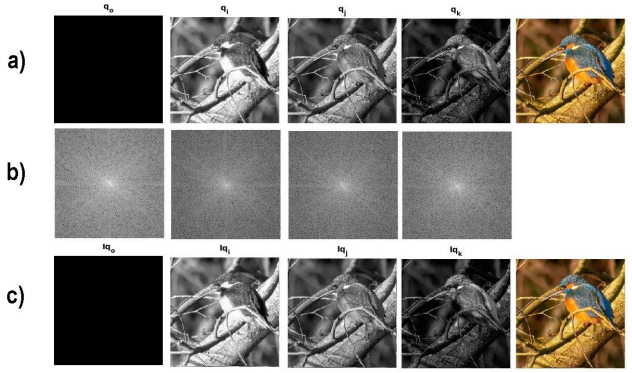

FIGURE 7. Quaternion Fourier transform (QFT) with Euclidean metric and its inverse of a quaternion image: a) the quaternion image and the original image; b) QFT; c) the inverse of QFT and the reconstructed image via the inverse of the QFT.

where A' is known as the *simplex part* and B' as the *perplex part*. The simplex part is the luminance component of the image and is purely imaginary, for this case only requires the H' image. The perplex part is the chrominance component. μ_1 and μ_2 are two arbitrary unit pure quaternions, where the multiplication between them generates a third $\mu_3 = \mu_1\mu_2$ quaternion, where $\mu_1\mu_2 \neq \mu_2\mu_1$. Note that μ_1, μ_2 and μ_3 form a new coordinate system isomorphic to $\boldsymbol{i}, \boldsymbol{j}$ and $\boldsymbol{k}$, but not constrained to the coordinate axes of 3-space.

$$H' = -\frac{1}{2}(Q\mu_1 + \mu_1 Q), \tag{64}$$

$$\begin{aligned} S' &= -\frac{1}{2}(Q\mu_2 + \mu_2 Q), \\ V' &= -\frac{1}{2}(Q\mu_3 + \mu_3 Q), \end{aligned} \tag{65}$$

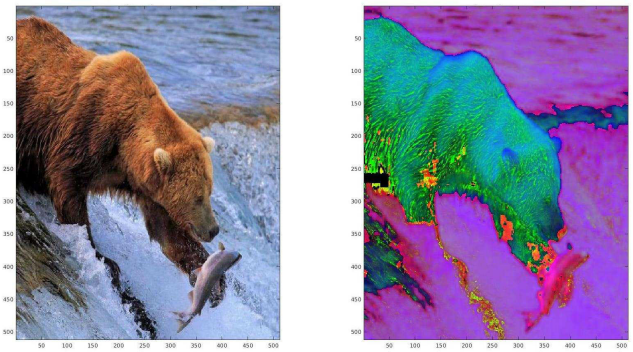

FIGURE 8. Image used for the construction of the symplectic form.

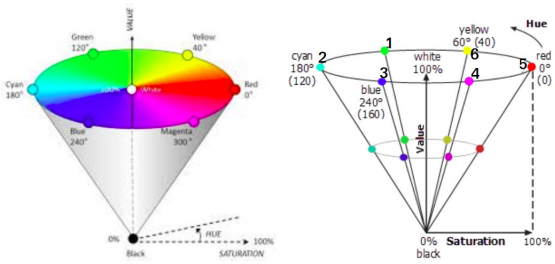

FIGURE 9. a) Cone of HSV model, b) color enumeration for identification with the sets of (μ_1, μ_2, μ_3).

where H', S' and V' are the components for the change of basis from $(\boldsymbol{i}, \boldsymbol{j}, \boldsymbol{k})$ to (μ_1, μ_2, μ_3).

C. THE FOURIER TRANSFORM FOR SYMPLECTIC FORM OF THE QUATERNION

In this subsection, we process the symplectic form using the quaternion split fast Fourier transform exposed in previous subsections. Similarly, as in the case of the symplectic form using the classical quaternion Fourier transform, the reader can see the results using the HSV Model based images.

The Fourier transform of the symplectic form can be formulated as follows

$$\mathcal{F}^{\pm L}[q'] = \mathcal{F}^{\pm L}[A'] + \mathcal{F}^{\pm L}[B']\mu_2 \tag{66}$$

$$\mathcal{F}^{\pm R}[q'] = \mathcal{F}^{\pm R}[A'] + \mathcal{F}^{\pm R}[B']\mu_2 \tag{67}$$

D. CONSTRUCTING THE SYMPLECTIC FORM OF AN IMAGE

Using the image shown in Figure 8, we obtain the symplectic form of the images for different sets of (μ_1, μ_2, μ_3), which allows us to select a specific color in the cone of the HSV model, see Figure 9. The results and the respective sets of (μ_1, μ_2, μ_3) are shown in figure 10. A' is the simplex part and B' is the perplex part, and Q corresponds to the sum of the simplex part and perplex part, as given by equation (63).

E. IMPLEMENTATION OF THE FOURIER TRANSFORM FOR SYMPLECTIC FORM OF THE QUATERNION

Figure 11 shows the Fourier transform for the symplectic forms shown in Figure 10. $QSFT(A')$, $QSFT(B')$, and

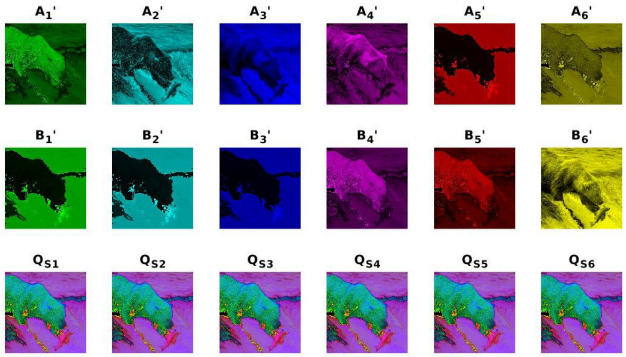

FIGURE 10. Symplectic form of the image. Using different sets of (μ_1, μ_2, μ_3), where each colour is shown as column 1-Green: $\mu_1 = -(1\boldsymbol{i})\boldsymbol{j}$, $\mu_2 = (1\boldsymbol{i})\boldsymbol{i}$, $\mu_3 = (1)\boldsymbol{k}$ 2-Cyan: $\mu_1 = (1)\boldsymbol{j} + (\sqrt{2})\boldsymbol{k}$, $\mu_2 = (1)\boldsymbol{j} - (\sqrt{2})\boldsymbol{k}$, $\mu_3 = (2\sqrt{2}\boldsymbol{i})\boldsymbol{k}$ 3-Blue: $\mu_1 = (1)\boldsymbol{k}$, $\mu_2 = -(1\boldsymbol{i})\boldsymbol{j}$, $\mu_2 = -(1\boldsymbol{i})\boldsymbol{i}$ 4-Magenta: $\mu_1 = (1)\boldsymbol{i} + (\sqrt{2})\boldsymbol{k}$, $\mu_2 = (1)\boldsymbol{i} - (\sqrt{2})\boldsymbol{k}$, $\mu_3 = (-2\sqrt{2})\boldsymbol{j}$ 5-Red: $\mu_1 = -(1\boldsymbol{i})\boldsymbol{i}$, $\mu_2 = (1)\boldsymbol{k}$, $\mu_1 = -(1\boldsymbol{i})\boldsymbol{j}$ 6-Yellow: $\mu_1 = -(\frac{1\boldsymbol{i}}{\sqrt{2}})\boldsymbol{i} - (\frac{1\boldsymbol{i}}{\sqrt{2}})\boldsymbol{j}$, $\mu_2 = -(\frac{1\boldsymbol{i}}{\sqrt{2}})\boldsymbol{i} + (\frac{1\boldsymbol{i}}{\sqrt{2}})\boldsymbol{j}$, $\mu_3 = (1)\boldsymbol{k}$.

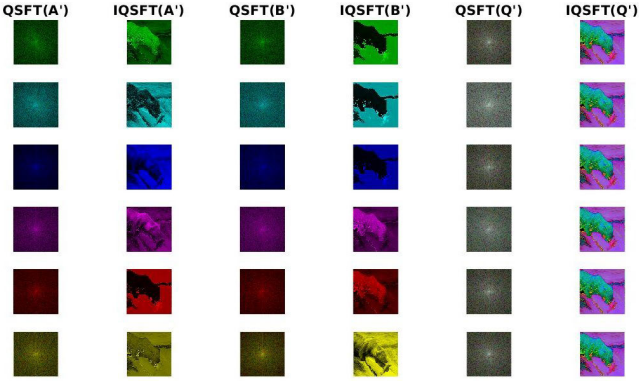

FIGURE 11. Implementation of the quaternion Split Fast Fourier Transform for the symplectic form of the image shown in Figure 10, where A' is the simplex part, B' is the perplex part, Q' is the sum of the equation 63, QSFT is the split fast Fourier transform, and IQSFT is the inverse.

$QSFT(B')$ are the quaternion Split Fast Fourier transform of the simplex part, perplex part, and according to the equation (63) the sum of the simplex and perplex parts, and $IQSFT$ corresponds to the inverse quaternion Split Fast Fourier transform.

V. INTERPOLATION USING SPLIT MOTORS OF THE CONFORMAL GEOMETRIC ALGEBRA $G_{4,1}$

The linearized RGB and CIEXYZ are vector spaces, with their values relative to light in the scene or real-world; but not uniform relative to human perception. In contrast, the HSV and HSL cone models are transformations of Cartesian RGB primaries (usually sRGB), and their components and colorimetry are relative to the color space from which they are derived. HSV also known as HSB is often utilized by artists, because it appears more natural to think and handle color in terms of hue and saturation than in terms of the subtraction or addition of color components. In this regard, in this section, we show the results of interpolating artificial

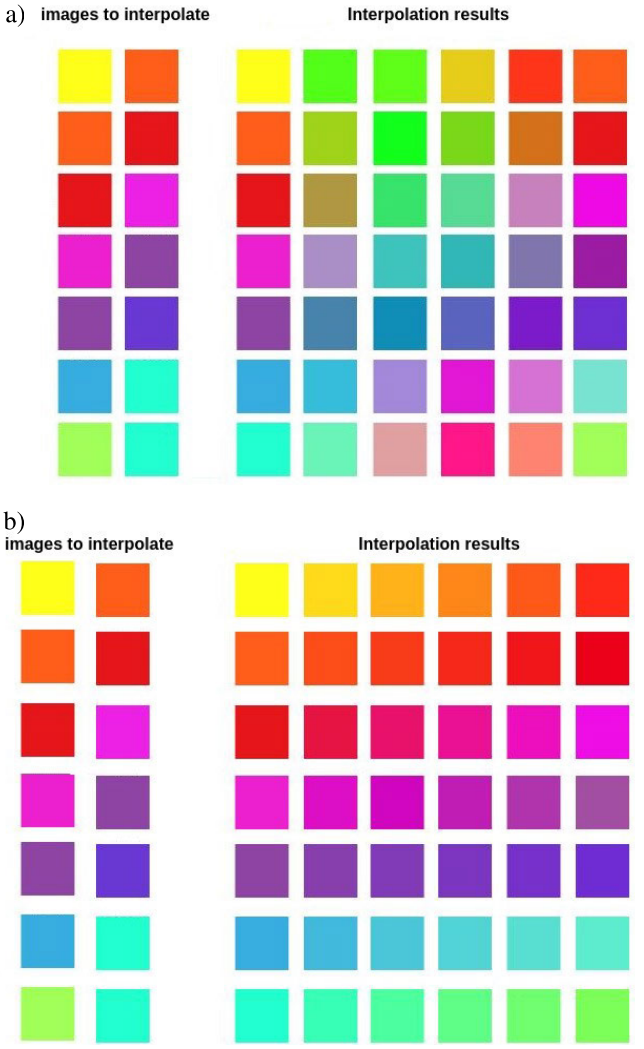

FIGURE 12. Seven pairs of changes of color image pixels: a) interpolated using the Euclidean metric in the $\mathbb{R}^3$; b) interpolated using Mikowski (space-time) metric in the HSV cone model.

and real color images using the RGB model and the HSV cone model. We show that the interpolation of color images using the HSV model is better and it behaves similarly to the human perception.

The HSV space will be represented in a pseudo-Euclidean space $\mathbb{R}^{3,1}$, see Figure 9. We select the split motors of the conformal geometric algebra $\boldsymbol{M}_s \in G_{4,1}$ to represent the Lorentz transformation which acts on the HSV model cone leaving the space-time metric invariant. The split motors are explained in subsection II-G.

In this section, we present the interpolation of two images with variations in brightness. For this purpose, we consider each pixel of the image as a point to be interpolated. The two points to be interpolated are located in the same position in both images. Each point is represented by the A_o and B_o respectively, see Figure 14.a.

$$A_o = (A_H, A_S, A_V),$$
$$B_o = (B_H, B_S, B_V), \tag{68}$$

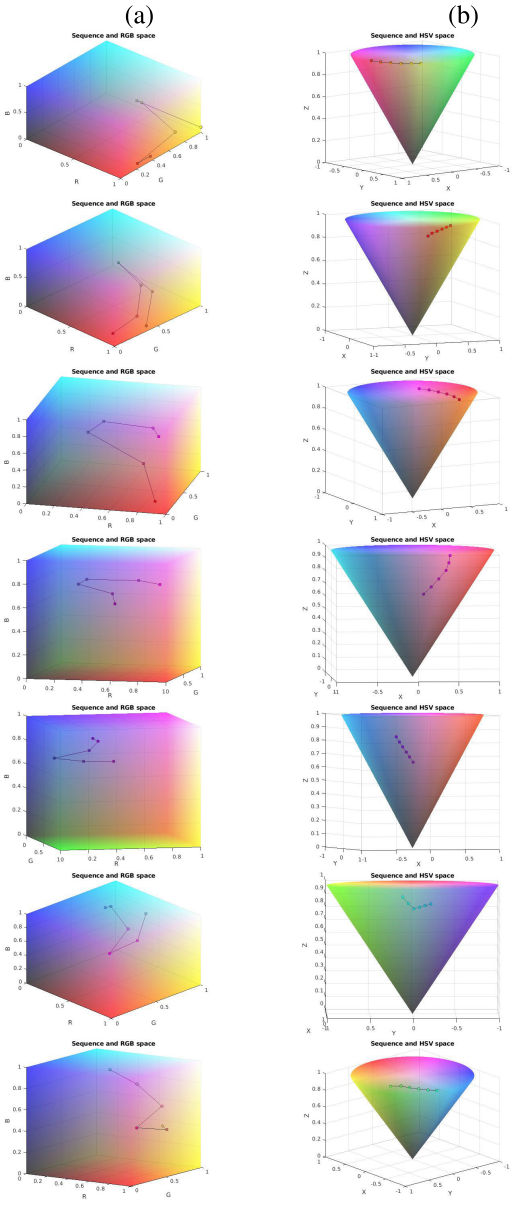

FIGURE 13. First experiment: the seven interpolated changes of color image pixels represented: column (a) in the RGB $\mathbb{R}^3$ space; column (b) in the HSV cone model.

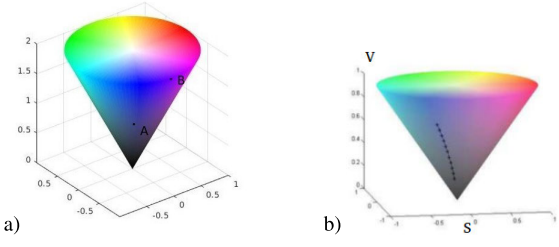

FIGURE 14. a) Graphical representation of two points on the cone. b) Scheme of the interpolation points on the cone ($\delta = 0.1, 0.2, \ldots, 1$).

Step1. We express the point A_o as a bivector

$$\boldsymbol{A}_o = A_H e_{15} + A_S e_{25} + A_V e_{12} \tag{69}$$

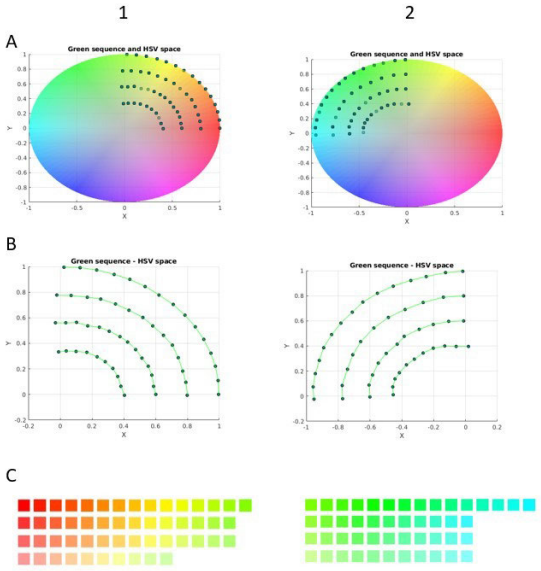

FIGURE 15. Second experiment: A) representation of the interpolated points on the cone with S = 1 and V = 1. (Interpolation over the quadrant 1 and 2). B) representation of the interpolating points. C) The colors obtained by the interpolation are represented in A) and B), each arch represents the interpolation between the first and last image of the arch. On each arch the point sequence is counterclockwise.

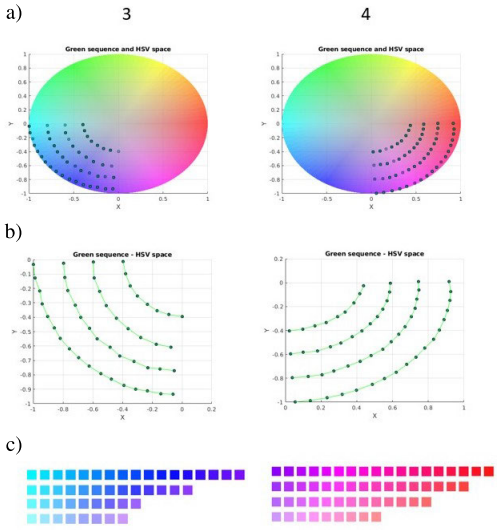

FIGURE 16. Third experiment: A) representation of the interpolated points on the cone with S = 1 and V = 1. (Interpolation over the quadrants 3 and 4). B) representation of the interpolated points. C) the colors obtained by the interpolation are represented in A and B, each arch represents the interpolation between the first and last image in the arch. On each arch the point sequence is counterclockwise.

Step 2. We get the translator to carry out the translation between the points

$$\boldsymbol{T} = \delta\rho\,(\cos(\psi)e_{15} + \sin(\psi)e_{25})) + \delta z e_{12} \tag{70}$$

where:

$$\psi = \delta\theta + \phi, \quad \delta = [0, 1]$$
$$\vec{A} = \vec{A_H} + \vec{A_S}, \quad \vec{B} = \vec{B_H} + \vec{B_S},$$

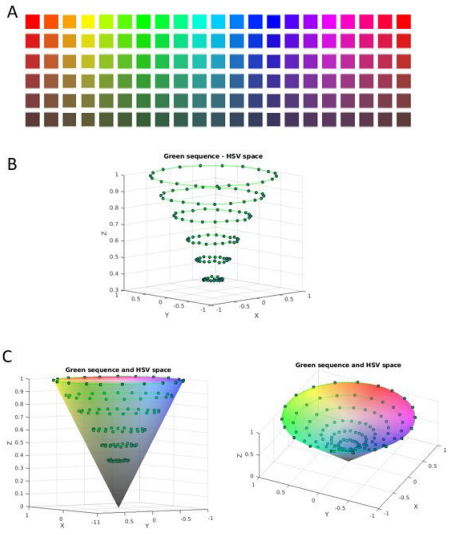

FIGURE 17. Fourth experiment: A) in each circle, it is shown the colors obtained by the interpolation between the first and last image in the row. B) representation of the points resulting from the interpolation. C) representation of the interpolated points on the cone with different perspectives.

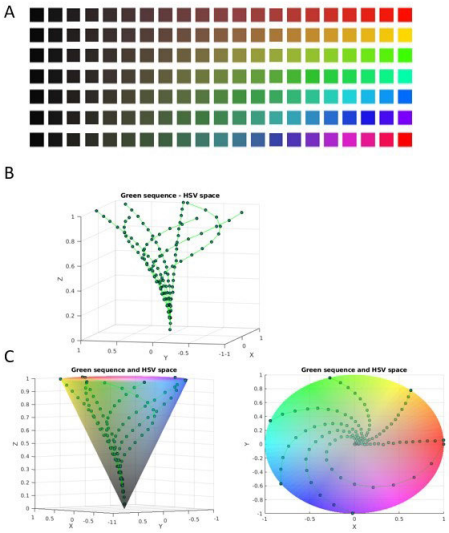

FIGURE 18. Fifth experiment: A) in each row, it is shown the colors obtained by the interpolation between the first and last image in the row. B) representation of the points resulting from the interpolation. C) representation of the points resulting from the interpolation over the cone with different perspectives.

$$\theta = \frac{\vec{A}\cdot\vec{B}}{|\vec{A}||\vec{B}|}, \quad \phi = cos^{-1}\left(\frac{A_H}{|A|}\right)$$
$$z = B_V - A_V, \quad \rho = |\vec{B}| - |\vec{A}|, \tag{71}$$

δ represents the interpolation step which yields a certain number of interpolated points, see Figure 14.b.

Step 3. We formulate the split rotor rotation for the rotation between the points:

$$\boldsymbol{R}_S = \cos\left(\frac{\delta\theta}{2}\right) + \sin\left(\frac{\delta\theta}{2}\right)e_{12}. \tag{72}$$

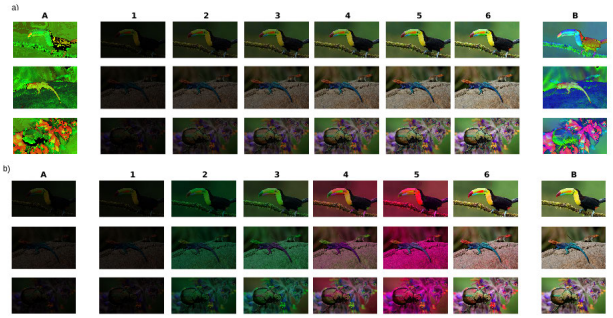

FIGURE 19. Sixth experiment 1: a) A and B are the images used for carrying out the interpolation. The numbered images are the result of the interpolation. b) A and B are the images used for carrying out the interpolation. We use the images in RGB format and the Euclidian metric.

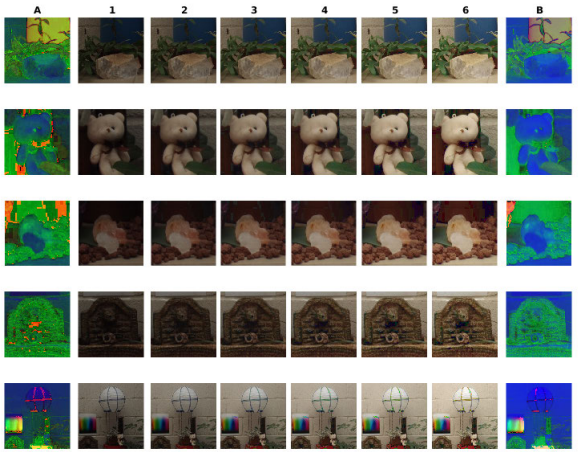

FIGURE 20. Sixth experiment 2: A and B are the images used for carrying out the interpolation. Images A and B were taken at different times of the day. The numbered images are the result of the interpolation. We use the images in HSV format and the Minkowski metric. For the visualization, the results are converted to RGB format.

Step 4. The translator is given by

$$\boldsymbol{T} = 1 + e_\infty \frac{\boldsymbol{t}}{2}, \tag{73}$$

where the translation is expressed as a bivector $\boldsymbol{t} = t_x e_{12} + t_y e_{23} + t_z e_{12}$.

Step 5. Considering the Equations (72) and (73), the split motor for the interpolation is given by

$$\boldsymbol{M}_S = \boldsymbol{T}\boldsymbol{R}_S \tag{74}$$

Step 6. Interpolation:

$$\boldsymbol{A}'_o = \boldsymbol{M}\boldsymbol{A}_o\tilde{\boldsymbol{M}} \tag{75}$$

To show the performance of the model proposed, we present next to a series of experimental results.

- First experiment: seven pairs of colors were interpolated to compute four images in between. You can see in Figure 12.a that the interpolation using Euclidean metric in the RGB $\mathbb{R}^3$ space and in Figure 12.b the interpolation using Mikowski (space-time) metric in the HSV cone model, here the results are converted to the RGB euclidean metric to visualize better in the color changes. Furthermore, these results are presented in the RGB $\mathbb{R}^3$ space in Figure 13.a and the interpolation using Minkowski (space-time) metric in the HSV cone model as shown in Figure 13.b. You can see that the sequences of the color pixels in the RGB $\mathbb{R}^3$ space don't follow smooth paths, in contrast, those color pixels in the HSV cone model follow rather smooth paths. This confirms that the interpolation of color images has to be done pixel-wise using the Minkowski (space-time) metric in the HSV cone model.
- The second experiment consists of the interpolation for four different values of saturation, with Value max (V = 1), considering that it covers the whole range of hue. The point sequence on each arch is counterclockwise. For this experiment, the cone was divided into four quadrants, and the interpolation was between points with different values of hue for each quadrant, with the same saturation and same Value, see Figure 15.
- The third experiment consists of the interpolation of nine points that have the next values (S = 0.1, 0.2, 0.3, 0.4, 0.5, 0.6, 0.7, 0.8 and 0.9, H = 1°, V = 1) with the point (H = 360°, S = 1, V = 1), see Figure 16.
- The fourth experiment consists of the interpolation of five pairs of points. The saturation (S) and value (V) have the same value in the pair of points, but the

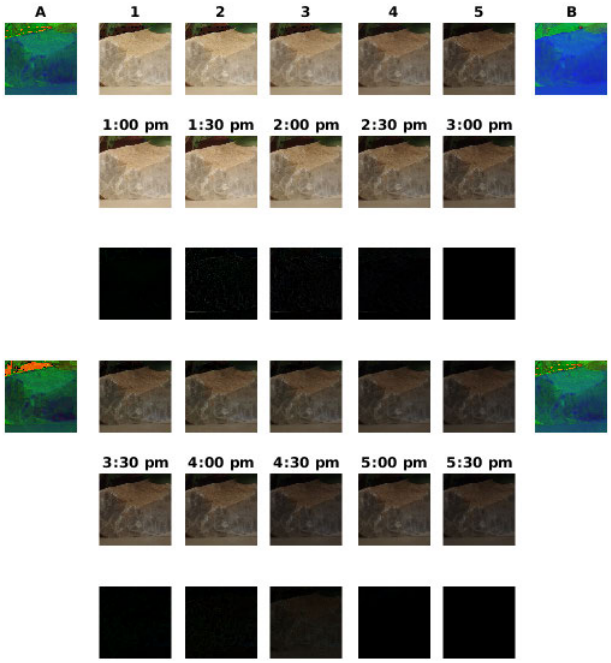

FIGURE 21. Sixth experiment 3: (first and quarter row) A and B are the images used for carrying out the interpolation using the RGB Euclidean metric. Images A and B were taken at different times of the day. The numbered images are the result of the interpolation. (second and fifth row) The images are the images taken every 30 minutes, starting at 1.00 pm and ending at 5.30 pm. (third and sixth row) The images represent the subtraction of the images obtained by interpolation and the images taken with the camera.

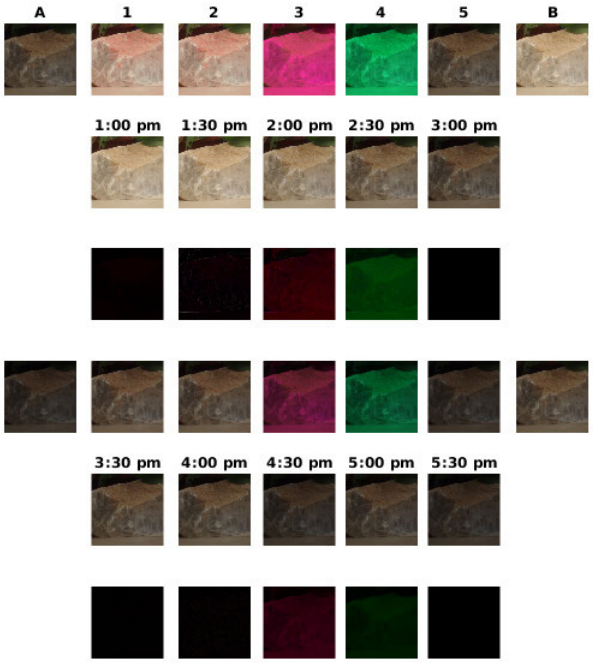

FIGURE 22. Sixth experiment 4: (first and quarter row) A and B are the images used to carry out the interpolation using the HSV Minkowski metric and the results are converted to RGB for visualization. The images A and B were taken at different times of the day. The numbered images are the result of the interpolation. (second and fifth row) The images are the images taken every 30 minutes, starting at 1.00 pm and ending at 5.30 pm. (third and sixth row) The images represent the subtraction of the images obtained by interpolation and the images taken with the camera.

value of Hue (H) is 1° for one of the points and 360° for the other, see Figure 17.

- The fifth experiment consists of the interpolation of the point (H =1°, S = 0.1, V= 0.1) with each of the seven points (H = 1°, 55°, 110°, 165°, 220°, 265°, and 360°, S = 1, V = 1), see Figure 18.
- The sixth experiment consists of four cases of the interpolation of two images that were taken at different times of the day, see Figures 19, 20, 21, 22.

We show in all the experiments that the processing of RGB images using the Euclidean metric in the $\mathbb{R}^3$ does not yield good results. In contrast, the experiments show using color synthetic images and images that change by daylight, that the color change follows the action of the Lorentz Lie group, thus the interpolation using the HSV Minkowski metric outperforms definitively the interpolation using RGB Euclidean metric.

VI. CONCLUSION

The authors present a complete study of the different mathematical methods to model the color phenomena and a new method to process color images. Our main contribution is to propose the correct metric to process color images using the Minkowski or space-time metric. The authors present a new model for representing and processing color using split quaternions and space-time conformal geometric algebra and propose two novel algorithms for practical color image processing: we formulate the novel (space-time) Split Quaternion Fourier Transform for color image processing and we interpolate color images processing using Split Motors which belong to the space-time conformal geometric algebra. We present successful applications of the Quaternion Split Fourier Transform and the interpolation processing. The experimental part proves with synthetic and real images that the color images have to be processed in the HSV cone model. We carry out a thorough comparison of these computations using the RGB metric in the $\mathbb{R}^3$ space and using the Minkowski metric in the HSV cone model. These comparisons show that the color image processing using the Minkowski metric in the HSV cone model ensures the quality of the enhanced colors near the quality of the cognitive perception of colors.

REFERENCES

[1] A. Ashtekar, A. Corichi, and M. Pierri, "Geometry in color perception," in *Black Holes, Gravitational Radiation and the Universe*. Berlin, Germany: Springer, 1999, pp. 535–550.
[2] J. C. Baez, "Division algebras and quantum theory," *arXiv:1101.5690* 2011.
[3] E. Bayro-Corrochano, *Geometric Computing for Wavelet Transforms, Robot Vision, Learning, Control, and Action*. London, U.K.: Springer, 2010.
[4] E. Bayro-Corrochano, *Geometric Algebra Applications Vol. I: Computer Vision, Graphics and Neurocomputing*. London, U.K.: Springer, 2019.
[5] J. C. Baez, "The octonions," *Bull. Amer. Math. Soc.*, vol. 39, no. 2, pp. 145–205, 2002.
[6] M. Berthier, "Geometry of color perception. Part 2: Perceived colors from real quantum states and Hering's rebit," *J. Math. Neurosci.*, vol. 10, no. 1, p. 14, Dec. 2020.
[7] M. Berthier, V. Garcin, N. Prencipe, and E. Provenzi, "The relativity of color perception," *J. Math. Psychol.*, vol. 103, Aug. 2021, Art. no. 102562.
[8] M. Berthier and E. Provenzi, "Quantum measurement and color perception: Theory and applications," *Proc. Roy. Soc. A*, vol. 478, no. 2258, 2022, Art. no. 20210508.
[9] A. R. Smith, "Color gamut transform pairs," *ACM SIGGRAPH Comput. Graph.*, vol. 12, no. 3, pp. 12–19, Aug. 1978.
[10] M. Calvo and J. M. Oller, "A distance between multivariate normal distributions based in an embedding into the Siegel group," *J. Multivariate Anal.*, vol. 35, no. 2, pp. 223–242, Nov. 1990.
[11] C. Chevalley, "The algebraic theory of spinors and Clifford algebras," in *Collected Works of Claude Chevalley*, vol. 2. Berlin, Germany: Springer, 1996.
[12] J. Cockle, "On systems of algebra involving more than one imaginary," *Phil. Mag.*, vol. 35, pp. 434–435, Jan. 1849.
[13] F. R. Cohen, "On whitehead squares, Cayley–Dickson algebras, and rational functions," *Soc. Mat. Mexicana*, vol. 37, pp. 55–62, Jan. 1992.
[14] J. Faraut and A. Koranyi, *Analysis on Symmetric Cones*. New York, NY, USA: Oxford, 1994.
[15] O. Ghorbel, W. Ayedi, M. W. Jmal, and M. Abid, "Images compression in WSN: Performance analysis," in *Proc. IEEE 14th Int. Conf. Commun. Technol.*, Nov. 2012, pp. 1363–1368.
[16] A. Guennec, N. Prencipe, and E. Provenzi, "Color correction with Lorentz boosts," in *Proc. 4th Int. Conf. Image Graph. Process.*, Sanya, China, Jan. 2021, pp. 1–12.
[17] M. Gogberashvili, "Split quaternions and particles in (2+1)-space," *Eur. Phys. J. C*, vol. 74, no. 12, p. 3200, Dec. 2014.
[18] H. Grassmann, "Theorie der farbenmischung," *Poggendorffs Annales der Physik*, vol. 89, pp. 69–84, Jan. 1853.
[19] H. von Helmholtz, "Versuch einer erweiterten anwendung des fechnerschen gesetzes im farbensystem," *Zeitschrift, Psychol. Physiol. Sinnesorg*, vol. 2, pp. 1–30, Jan. 1891.
[20] E. Hitzer, "The orthogonal planes split of quaternions and its relation to quaternion geometry of rotations," *J. Phys., Conf. Ser.*, vol. 597, Apr. 2015, Art. no. 012042.

[21] P. Jordan, N. J. Von, and E. Wigner, "On an algebraic generalization of the quantum mechanical formalism," *Annu. Math.*, vol. 35, pp. 29–64, Jan. 1934.
[22] C. N. Ganavi and A. A. Khan, "Performance evaluation of 3D image compression techniques," in *Proc. 2nd Int. Conf. Signal Process., Image Process. VLSI*, 2015, pp. 447–450.
[23] D. H. Krantz, "Color measurement and color theory: I. representation theorem for Grassmann structures," *J. Math. Psychol.*, vol. 12, no. 3, pp. 283–303, Aug. 1975.
[24] A. D. Logvinenko, "The geometric structure of color," *J. Vis.*, vol. 15, no. 1, p. 16, Jan. 2015.
[25] Y. Li, M. Wei, F. Zhang, and J. Zhao, "A fast structure-preserving method for computing the singular value decomposition of a quaternion matrix," *Appl. Math. Comput.*, vol. 235, pp. 157–167, Oct. 2014.
[26] W. R. Hamilton, *Elements of Quaternions*. London, U.K.: Longmans Green, 1969.
[27] W. A. Jassim, R. Mukundan, and P. Raveendran, "New orthogonal polynomials for speech signal and image processing," *IET Signal Process.*, vol. 6, no. 8, pp. 713–723, Oct. 2012.
[28] B. M. Mahmmod, S. H. Abdulhussain, T. Suk, and A. Hussain, "Fast computation of Hahn polynomials for high order moments," *IEEE Access*, vol. 10, pp. 48719–48732, 2022.
[29] J. C. Maxwell, "On color vision," *Proc. Roy. Inst. Great Britain*, vol. 6, pp. 260–271, Jan. 1872.
[30] K. McCrimmon, "Jordan algebras and their applications," *Bull. Amer. Math. Soc.*, vol. 84, pp. 612–627, Jan. 1978.
[31] K. McCrimmon, *A Taste of Jordan Algebras*. New York, NY, USA: Springer, 2004.
[32] M. Özdemir and A. A. Ergin, "Rotations with unit timelike quaternions in Minkowski 3-space," *J. Geometry Phys.*, vol. 56, no. 2, pp. 322–336, Feb. 2006.
[33] M. Özdemir, "The roots of a split quaternion," *Appl. Math. Lett.*, vol. 22, pp. 258–263, Jan. 2009.
[34] S. S. Patterson, M. Neitz, and J. Neitz, "Reconciling color vision models with midget ganglion cell receptive fields," *Frontiers Neurosci.*, vol. 13, p. 865, Aug. 2019.
[35] N. Prencipe, V. Garcin, and E. Provenz, "Origins of hyperbolicity in color perception," *J. Imag.*, vol. 6, no. 1, pp. 1–42, 2020.
[36] E. Provenzi, "Geometry of color perception. Part 1: Structures and metrics of a homogeneous color space," *J. Math. Neurosci.*, vol. 10, no. 1, pp. 1–16, Dec. 2020.
[37] E. Reinhard, K. E. Arif, A. A. Oguz, and G. Johnson, *Color Imaging, Fundamentals and Applications*. Wellesley, MA, USA: AK Peters, 2008.
[38] H. L. Resnikoff, "Differential geometry and color perception," *J. Math. Biol.*, vol. 1, no. 2, pp. 97–131, Sep. 1974.
[39] B. Riemann, *Über Die Hypothesen, Welche Der Geometrie zu Grunde Liegen*. New York, NY, USA: Dover, 1953.
[40] S. J. Sangwine, "Fourier transforms of colour images using quaternion or hypercomplex, numbers," *Electron. Lett.*, vol. 32, no. 21, p. 1979, 1996.
[41] T. A. Ell, B. N. Le, and S. J. Sangwine, *Quaternion Fourier Transforms for Signal and Image Processing*. Hoboken, NJ, USA: Wiley, 2014.
[42] E. Schrödinger, "Grundlinien einer theorie der farbenmetrik in tagessehen," *Annalen Physik*, vol. 63, no. 21, pp. 397–520, 1920.
[43] C. L. Siegel, "Symplectic geometry," *Amer. J. Math.*, vol. 65, pp. 1–86, Jan. 1943.
[44] R. L. de Valois and K. K. de Valois, "Neural coding of color," in *Readings on Color: The Science of Color*, A. Byrne and D. R. Hilbert, Eds. Cambridge, MA, USA: MIT Press, 1997, pp. 93–140.
[45] H. Yilmaz, "Color vision and a new approach to general perception," in *Biological Prototypes and Synthetic Systems*. Boston, MA, USA: Springer, 1962, pp. 126–141.
[46] H. Yilmaz, "On color perception," *Bull. Math. Biophys.*, vol. 24, pp. 5–29, 1962.
[47] J. W. Weinberg, "The geometry of colors," *Gen. Relativity Gravitation*, vol. 7, no. 1, pp. 135–169, Jan. 1976.
[48] H. Weyl, "Mind and nature," in *Mind and Nature, Selected Writings on Philosophy, Mathematics, and Physics*. Princeton, NJ, USA: Princeton Univ. Press, 2009.
[49] G. Wyszecki and G. Stiles, *Color Science, Concepts and Methods, Quantitative Data and Formulae*. New York, NY, USA, Wiley, 2000.

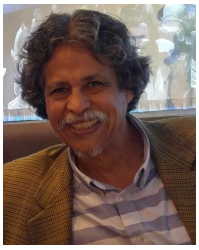

EDUARDO BAYRO-CORROCHANO (Senior Member, IEEE) received the Ph.D. degree in systems engineering from the University of Wales, Cardiff, in 1994. From 1995 to 1999, he was a Researcher and a Lecturer with the Institute for Computer Science, Christian-Albrecht University of Kiel, Germany, where he was involved in applications of geometric Clifford algebra to cognitive systems. In August 2007, he was a DFG Mercator Guest Professor with the KIT, Technische Hochschule Karlsruhe, Germany. From 2014 to 2015, he was a Visiting Full Professor with the Media Laboratory, Massachusetts Institute of Technology (MIT), Boston, MA, USA. He is currently a Full Professor in geometric cybernetics with the Department of Electrical Engineering and Computer Science, CINVESTAV, Campus Guadalajara, Jalisco, Mexico. He is the author of seven Springer Verlag books and published more than 230 refereed journal articles, book chapters, and conference papers. He is a fellow of the International Association of Pattern Recognition Society and the Asian Artificial Intelligence Association. He is an Associate Editor of the *Journal of Robotica* and an Editor of the ICRA Conference. He was an Associate Editor of the IEEE TRANSACTIONS ON NEURAL NETWORKS AND LEARNING SYSTEMS, *Journal of Mathematical Imaging and Vision*, and *Pattern Recognition*. He was the General Chair of ICPR2016 in December, Cancún, Mexico, and IEEE/RAS Humanoids 2016 in November, Cancún.

ZULEIMA VAZQUEZ-FLORES received the bachelor's degree in physics and the M.Sc. degree in optics from the Centro de Investigaciones en Óptica (CIO), León, Guanajuato, Mexico, in 2015 and 2018, respectively. She is currently pursuing the Ph.D. degree with the CINVESTAV, Campus Guadalajara, Mexico. She is involved in the theory and applications of the quaternion split Fourier transform, quantum quaternion Fourier transform, quaternion fractional transform, and quaternion Radon transform. Her research interests include signal and image processing, and artificial intelligence.

ULISES URIOSTEGUI-LEGORRETA received the bachelor's degree in mathematical physics and the M.Sc. degree in engineering physics from the Michoacan University of Saint Nicholas of Hidalgo (UMSNH), in 2013, and the Ph.D. degree in computer science and electrical engineering from the Center of Research and Advanced Studies, CINVESTAV, Campus Guadalajara, Mexico, in 2020. He is currently pursuing the Ph.D. degree in science with the Department of Physics Engineering, UMSNH. His research interests include modeling, dynamics, control, and chaos of dynamic systems.